

# Spin-orbit torques and magnetization switching in Gd/Fe multilayers generated by current injection in NiCu alloys

Federica Nasr,<sup>1</sup> Federico Binda,<sup>1</sup> Charles-Henri Lambert,<sup>1</sup> Giacomo Sala,<sup>1</sup> Paul Noël,<sup>1</sup> and Pietro Gambardella<sup>1</sup>  
*Department of Materials, ETH Zurich, CH-8093 Zurich, Switzerland*

(\*Authors to whom correspondence should be addressed: federica.nasr@mat.ethz.ch, pietro.gambardella@mat.ethz.ch)

(Dated: 29 December 2023)

Light transition metals have recently emerged as a sustainable material class for efficient spin-charge interconversion. We report measurements of current-induced spin-orbit torques generated by  $\text{Ni}_{1-x}\text{Cu}_x$  alloys in perpendicularly-magnetized ferrimagnetic Gd/Fe multilayers. We show that the spin-orbit torque efficiency of  $\text{Ni}_{1-x}\text{Cu}_x$  increases with the Ni/Cu atomic ratio, reaching values comparable to those of Pt for  $\text{Ni}_{55}\text{Cu}_{45}$ . Furthermore, we demonstrate magnetization switching of a 20-nm-thick Gd/Fe multilayer with a threshold current that decreases with increasing Ni concentration, similar to the spin-orbit torque efficiency. Our findings show that  $\text{Ni}_{1-x}\text{Cu}_x$ -based magnetic heterostructures allow for efficient control of the magnetization by electric currents.

Materials that allow for converting charge currents into spin currents are used to generate spin-orbit torques (SOTs) in different classes of magnetic systems and devices.<sup>1</sup> SOTs enable the energy-efficient manipulation of the magnetization in ferromagnets,<sup>2-4</sup> ferrimagnets,<sup>5-8</sup> and antiferromagnets,<sup>9-11</sup> with applications in magnetic random access memories,<sup>12</sup> racetrack memories,<sup>13</sup> logic devices,<sup>14</sup> and spin-torque nanos oscillators.<sup>15,16</sup> SOTs have been extensively studied in heavy metal/ferromagnet bilayers,<sup>1-3,17-21</sup> where the charge-to-spin conversion originates from the interplay of bulk and interfacial spin-orbit coupling, as exemplified by the spin Hall<sup>22</sup> and Rashba-Edelstein effects.<sup>23</sup> The two figures of merit describing the charge-to-spin conversion efficiency are the spin Hall angle and the spin Hall conductivity. The former is defined as the ratio of the transverse spin current generated in the spin injector to the applied charge current, whereas the latter is the ratio of the spin current to the external electric field driving the charge current.<sup>1,24</sup>

A large spin Hall angle ( $\geq 0.1$ ) is usually observed in the  $5d$  transition metals, such as Ta, W, and Pt, owing to their strong atomic spin-orbit coupling.<sup>22</sup> Whether light metals can also show large charge-to-spin conversion is a question of both fundamental and practical impact on developing new and low-cost spin injector materials. In this context,  $3d$  transition metals and their alloys have recently attracted interest because they present appreciable spin Hall angles despite their weak spin-orbit coupling.<sup>25-31</sup> The interest in light metals has further surged following the theoretical prediction of a large orbital Hall conductivity in the nonmagnetic  $3d$  elements,<sup>32,33</sup> which can lead to the generation of strong SOTs in adjacent ferromagnetic layers.<sup>34-37</sup>

For transition metals, besides the spin-orbit coupling, the  $d$ -orbital occupation plays an important role in determining the magnitude and sign of the spin Hall angle.<sup>22,32</sup> Ni is particularly interesting in this respect because it has the same valency and a similar band structure as Pt. The calculated spin Hall conductivity of Ni is  $\sim 1.2 \times 10^5 \Omega^{-1}\text{m}^{-1}$ , about half of Pt, whereas the orbital Hall conductivities of Ni and Pt are very similar.<sup>33</sup> Extrinsic spin scattering effects due to alloying of different metallic elements can further enhance the charge-spin interconversion efficiency,<sup>38-41</sup> as shown, e.g.,

for  $\text{Cu}_{1-x}\text{Bi}_x$  and  $\text{Au}_{1-x}\text{Pt}_x$ .<sup>42,43</sup> In light of these observations, experimental work has focused on  $\text{Ni}_x\text{Cu}_{1-x}$  alloys, in which the introduction of Cu reduces the Curie temperature relative to pure Ni, making the alloy paramagnetic at room temperature for  $x \leq 70\%$ .<sup>44,45</sup> Despite the alloying, the band structure of  $\text{Ni}_x\text{Cu}_{1-x}$  remains similar to that of paramagnetic Ni, suggesting a significant intrinsic spin Hall effect regardless of chemical disorder.<sup>46</sup> Recent experiments have reported large effective spin Hall angles comparable to  $5d$  metals in Permalloy/ $\text{Ni}_{60}\text{Cu}_{40}$ , CoFeB/Cu/ $\text{Ni}_x\text{Cu}_{1-x}$ , and YIG/ $\text{Ni}_{80}\text{Cu}_{20}$  bilayers.<sup>46-48</sup> Additionally, spin-to-charge conversion in CoFeB/ $\text{Ni}_{70}\text{Cu}_{30}$  was shown to induce THz emission upon fs laser irradiation with intensity up to half that of CoFeB/Pt.<sup>49</sup>

These studies show that  $\text{Ni}_x\text{Cu}_{1-x}$  alloys constitute an interesting material system for spin-charge interconversion and the realization of spin current detectors. Here, we investigate  $\text{Ni}_x\text{Cu}_{1-x}$  alloys as spin injectors for generating SOTs in perpendicularly magnetized  $\text{Ni}_x\text{Cu}_{1-x}/\text{Ti}/[\text{Gd}/\text{Fe}]_{30}$  heterostructures. We select three different compositions ( $x = 40, 50, 55\%$ ) for which  $\text{Ni}_x\text{Cu}_{1-x}$  is paramagnetic at room temperature and report composition-dependent SOT efficiencies, reaching values of up to 0.06 for  $x = 55\%$ , which corresponds to a spin Hall conductivity of  $(1.04 \pm 0.07) \times 10^5 \Omega^{-1}\text{m}^{-1}$  without taking into account corrections due to spin memory loss and interface transparency. In addition, we demonstrate the efficient magnetization switching capability of these systems, including a fourth alloy's composition  $x = 70\%$  at the ferromagnetic phase transition. Our results show that  $\text{Ni}_x\text{Cu}_{1-x}$  alloys are efficient spin current generators that can be used to achieve electrical control of the magnetization in spintronic devices.

We fabricated three different sets of samples, all grown on  $\text{SiO}_2$  substrates by magnetron sputtering: (i) the full heterostructures  $\text{Ni}_x\text{Cu}_{1-x}(6\text{nm})/\text{Ti}(1\text{nm})/\text{FiM}/\text{Si}_3\text{N}_4$  ( $x = 40, 50, 55, 70\%$ ), referred to as  $\text{Ni}_x$ , where FiM stands for the ferrimagnetic multilayer  $[\text{Gd}(0.4\text{nm})/\text{Fe}(0.27\text{nm})]_{30}$ , (ii) the reference layers  $\text{Ni}_x\text{Cu}_{1-x}(6\text{nm})/\text{Si}_3\text{N}_4$ , referred to as  $\text{Ni}_x - r$ , and (iii) the single FiM layer  $\text{Ti}(1\text{nm})/\text{FiM}/\text{Si}_3\text{N}_4$ . The  $\text{Ni}_x\text{Cu}_{1-x}$  layers are amorphous, as revealed by X-ray diffraction. The  $\text{Ni}_x\text{Cu}_{1-x}$  layers in Ni40, Ni50, and Ni55

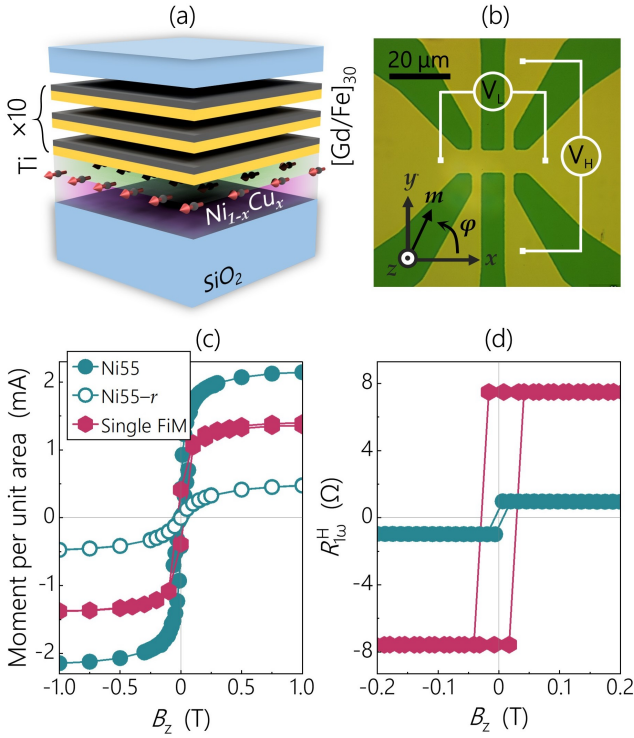


FIG. 1. (a) Schematic of the  $\text{Ni}_x$  heterostructure. (b) Optical image of a Hall bar device with superimposed electrical connections and coordinate system. (c) Magnetic moment per unit area as a function of out-of-plane magnetic field for Ni55 (green dots), its reference Ni55- $r$  (open circles), and the single FiM sample (purple hexagons). (d) Anomalous Hall resistance as a function of out-of-plane magnetic field for Ni55 (green dots) and the single FiM (purple hexagons). The current density in the FiM layer was  $j_{\text{FiM}} \sim 3.5 \times 10^{10} \text{ A/m}^2$  in both measurements.

are paramagnetic at room temperature, which avoids spurious magnetotransport signals in the electrical measurements of SOTs. The Ti layer in all the heterostructures serves as a spacer to suppress possible magnetic proximity effects between  $\text{Ni}_x\text{Cu}_{1-x}$  and the FiM. A sketch of the  $\text{Ni}_x$  samples is shown in Fig. 1(a). The samples were patterned in 7.5- $\mu\text{m}$ -wide and 11- $\mu\text{m}$ -long Hall bar devices using photolithography and lift-off, as shown in Fig. 1(b).

Figure 1(c) shows  $M_s t$ , the magnetic moment per unit area, as a function of out-of-plane magnetic field of Ni55, its reference Ni55- $r$ , and the single FiM sample. Here,  $M_s$  represents the saturation magnetization,  $t$  the thickness of the magnetic layer, and  $M_s t$  is the total magnetic moment of the as-grown layers measured at room temperature by a superconducting quantum interference device divided by the sample area. The comparison between the different curves shows that Ni55- $r$  develops a sizable magnetization in a magnetic field, which adds to that of the FiM in the Ni55 sample. Because we consider the effect of the SOTs on the sole FiM, we estimate an effective magnetic moment per unit area for each Ni $x$  sample as the difference between the moments of the full heterostructures Ni $x$  and their references Ni $x$ - $r$ , namely  $M_s t = (M_s t)_{\text{Ni}_x} - (M_s t)_{\text{Ni}_x-r}$ . The magnetotransport measure-

ments were performed by injecting an alternate current of frequency  $\omega/(2\pi) = 10\text{Hz}$  and density  $j$  and computing the respective Hall ( $R_{1,2\omega}^H$ ) and longitudinal ( $R_{1,2\omega}^L$ ) components of the first and second harmonic resistances from the measured harmonic voltages.<sup>18,50</sup> The first harmonic Hall resistance accounts for the contributions from the anomalous Hall effect (AHE) and planar Hall effect (PHE) and is given by

$$R_{1\omega}^H = R_{\text{AHE}} \cos \vartheta + R_{\text{PHE}} \sin^2 \vartheta \sin 2\varphi, \quad (1)$$

where  $R_{\text{AHE}}$  and  $R_{\text{PHE}}$  are the anomalous and planar Hall resistance coefficients, and  $\vartheta$  and  $\varphi$  are the polar and azimuthal angles between the magnetization and the  $z$ - and  $x$ -axis, respectively. Figure 1(d) shows  $R_{1\omega}^H$  as a function of out-of-plane field for Ni55 and the single FiM sample. The signal is dominated by the AHE of the FiM in both samples; the remanence and polarity of the curves indicate that the FiM has perpendicular magnetic anisotropy and its magnetization is Fe-like. The amplitude of the AHE in Ni55 is reduced compared to the single FiM sample because part of the current flows in the paramagnetic  $\text{Ni}_x\text{Cu}_{1-x}$  layer and Ni has opposite sign of  $R_{\text{AHE}}$  compared to Fe.<sup>51</sup> Moreover, the magnetic properties and AHE of FiM layers are known to depend on the adjacent layers, which are different in the two samples.<sup>52-55</sup>

The SOTs were measured using the harmonic Hall voltage method, which relies on  $R_{2\omega}^H$  as a measure of the current-induced oscillations of the magnetization.<sup>18,56</sup> The SOTs can be decomposed into two components orthogonal to the unitary magnetization  $\mathbf{m}$ , to define a damping-like (DL) torque,  $\mathbf{T}_{\text{DL}} = \tau_{\text{DL}} \mathbf{m} \times (\boldsymbol{\zeta} \times \mathbf{m})$ , and a field-like (FL) torque,  $\mathbf{T}_{\text{FL}} = \tau_{\text{FL}} \mathbf{m} \times \boldsymbol{\zeta}$ . Here, the torques are normalized by the magnetization,  $\boldsymbol{\zeta}$  is the unit vector representing the spin polarization of the injected spin current, and  $\tau_{\text{DL}}$  and  $\tau_{\text{FL}}$  are the amplitudes of the effective magnetic fields describing the action of the SOTs on the magnetization. We estimated  $\tau_{\text{DL}}$  and  $\tau_{\text{FL}+\text{Oe}}$ , with Oe denoting the Oersted field, using the following equations valid under the assumption  $\vartheta \rightarrow 0$ <sup>56</sup>

$$\tau_{\text{DL}} = 2 \frac{B_x \pm 2\chi B_y}{1 - 4\chi^2}, \quad (2)$$

$$\tau_{\text{FL}+\text{Oe}} = 2 \frac{B_y \pm 2\chi B_x}{1 - 4\chi^2}, \quad (3)$$

where  $\chi = R_{\text{PHE}}/R_{\text{AHE}}$  ( $\sim 10^{-2}$  in our samples) and  $B_{x,y} \equiv \left( \frac{\partial R_{2\omega}^H}{\partial H} / \frac{\partial^2 R_{1\omega}^H}{\partial^2 H} \right) \Big|_{\hat{m} \parallel x,y}$ . As an illustrative case, Figs. 2(a) and (b) show  $R_{1,2\omega}^H$  of Ni40 as a function of a nearly in-plane external magnetic field oriented along the  $x$ - and  $y$ -axes measured at  $j = 7.4 \times 10^{10} \text{ A/m}^2$  ( $j_{\text{NiCu}} = 1.9 \times 10^{11} \text{ A/m}^2$ ) and the fits (solid lines) used to estimate the SOT effective fields. Figure 2(c) shows  $\tau_{\text{DL}}$  and  $\tau_{\text{FL}+\text{Oe}}$  vs  $j_{\text{NiCu}}$  for the different Ni $x$  samples. Note that the total FL+Oe field is similar to the expected Oersted field from Biot-Savart's law, evidencing the small contribution of the FL torque in our samples.

The SOT efficiencies with respect to the applied current density ( $j$ ) and electric field driving the current ( $E$ ) are given

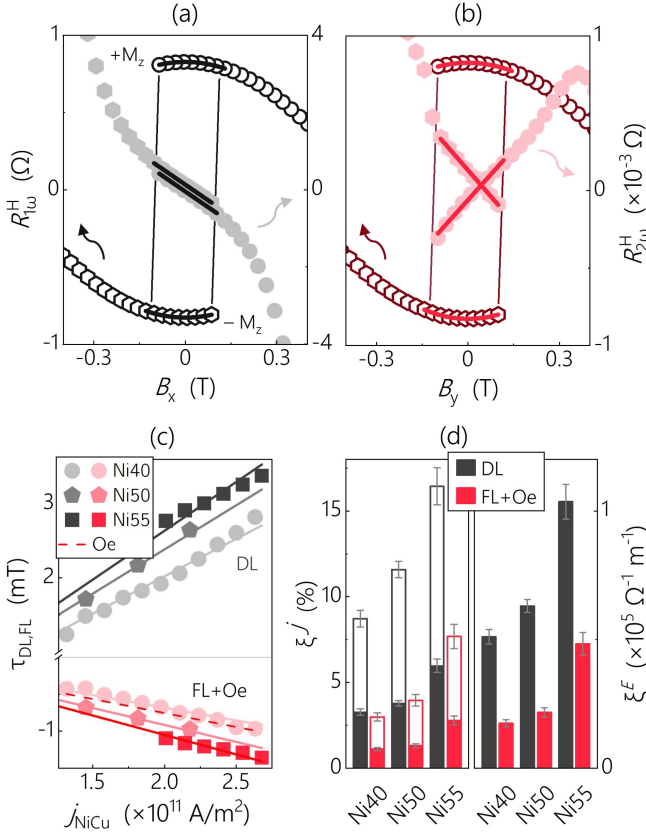


FIG. 2. (a) and (b)  $R_{1\omega}^H$  (left axis) and  $R_{2\omega}^H$  (right axis) of Ni40 as a function of external magnetic field applied at an angle  $\vartheta_B = 87^\circ$  along (a) the  $x$ -axis (left plot) and (b) the  $y$ -axis (right plot). The solid lines are fits used to estimate  $\partial^2 R_{1\omega}^H / \partial^2 H$  and  $\partial R_{2\omega}^H / \partial H$  in Eq. 3. (c) DL (black) and FL (red) effective fields of Ni40, Ni50, and Ni55 as a function of the current density in the  $Ni_xCu_{1-x}$  layer. The solid lines are linear fits with intercept forced to zero. The error bars, which include the fit errors in (a) and (b) and the uncertainties in  $R_{AHE}$  and  $R_{PHE}$ , are smaller than the symbols. (d) DL (black) and FL (red) SOT efficiencies of Ni $_x$ . The left panel shows the SOT efficiencies with respect to the total current density  $\xi^j$  (empty columns) and to the current density in the sole  $Ni_xCu_{1-x}$  layer,  $\xi^{j_{NiCu}}$  (full columns); the right panel shows the SOT efficiencies with respect to the electric field  $\xi^E$ . The errors are calculated from the uncertainty of the fits in (c) and  $M_s t$ .

by<sup>1,24</sup>

$$\xi_{DL,FL}^j = \frac{2e}{\hbar} M_s t \frac{\tau_{DL,FL}}{j}, \quad (4)$$

$$\xi_{DL,FL}^E = \frac{2e}{\hbar} M_s t \frac{\tau_{DL,FL}}{E}, \quad (5)$$

where  $e$  is the elementary charge and  $\hbar$  is the reduced Planck constant.  $\xi^j$  ( $\xi^E$ ) represents the ratio of the effective spin current absorbed by the magnetic layer relative to the applied charge current (electric field) and can be thus regarded as an effective spin Hall angle (effective spin Hall conductivity) for a specific combination of a spin injector and magnetic layer. Because distinguishing between SOTs generated by spin and orbital currents is not straightforward,<sup>37</sup>  $\xi^j$  and  $\xi^E$  include

also the effect of orbital currents. The efficiencies calculated by Eqs. 4 and 5 constitute a lower bound for quantifying the charge-to-spin conversion of a spin injector since they do not account for the spin transparency of the interface between the spin injector and the magnetic material.

Figure 2(d) presents the SOT efficiencies calculated by averaging over two devices for each Ni $_x$  sample. The sign of the DL torque is consistent with that of Pt/Co, considering the same stacking order between the spin injector and the magnetic layer. Both  $\xi_{DL}^j$  and  $\xi_{FL+Oe}^j$  increase monotonically with Ni content and reach a maximum at  $x = 55\%$  in the measured composition range:  $\xi_{DL}^j = 0.16$  ( $\xi_{DL}^E = 1.04 \times 10^5 \Omega^{-1}m^{-1}$ ) and  $\xi_{FL+Oe}^j = 0.08$  ( $\xi_{FL+Oe}^E = 0.48 \times 10^5 \Omega^{-1}m^{-1}$ ) at  $x = 55\%$  are comparable with the values reported for  $5d$  metal system such as Pt/Co.<sup>1</sup> In making such a comparison, one should note that the effective spin Hall angle changes if it is calculated with respect to the average current density ( $\xi^j$ ) or to the current density flowing in the spin injector ( $\xi^{j_{NiCu}}$ ) estimated using a parallel resistor model. In the latter case, we obtain  $\xi_{DL}^{j_{NiCu}} = 0.06$  and  $\xi_{FL+Oe}^{j_{NiCu}} = 0.03$ , which are about half of the values reported for Pt/Co. The resistivity and magnetization parameters used to calculate the different  $\xi$  are reported in Table I.

We now compare the SOT efficiencies of the Ni $_x$  samples with the measurements of spin-charge interconversion reported for  $Ni_xCu_{1-x}$  alloys in the literature. Keller *et al.*<sup>46</sup> reported  $\xi_{DL}^E \sim 1 \times 10^5 \Omega^{-1}m^{-1}$  at  $x = 60\%$ , before considering any correction due to interfacial spin memory loss. This efficiency, normalized by the reported electrical conductivity of the NiCu layer of  $1.93 \times 10^6 \Omega^{-1}m^{-1}$ , corresponds to a spin Hall angle of 0.05. Varotto *et al.*<sup>47</sup> reported a spin Hall angle of 0.04 at  $x = 60\%$ , in line with our results. Because the spin diffusion length  $\lambda_s$  decreases with increasing Ni content<sup>57</sup> and the measured values of  $\tau_{DL}$  and  $\tau_{FL}$  depend on  $\lambda_s$  if  $t_{NiCu} \lesssim 2\lambda_s$ , an alternative figure of merit is the product  $\xi^{j_{NiCu}} \lambda_s$ . Assuming  $\lambda_s \sim 4$  nm at  $x = 40\%$  and 3 nm at  $x = 55\%$ ,<sup>57</sup> we obtain  $\xi_{DL}^{j_{NiCu}} \lambda_s = 0.12$  nm for Ni40 and 0.18 nm for Ni55. These values are similar to  $\xi_{DL} \lambda_s = 0.1$  nm obtained in Ref. 47. Overall, this comparison shows that  $Ni_xCu_{1-x}$  alloys present large and comparable figures of merit for charge-to-spin and spin-to-charge conversion.

Sample	$M_s t$ (mA)	$R_{AHE}$ ( $\Omega$ )	$\rho$ ( $\mu\Omega$ cm)	$\rho_{NiCu}$ ( $\mu\Omega$ cm)	$\rho_{FiM}$ ( $\mu\Omega$ cm)	$R/R_{NiCu}$ (%)
Ni40	1.0	0.8	170	64	320	58
Ni50	1.1	0.7	181	60	423	67
Ni55	1.7	1.0	157	58	308	60
Ni70	2.9	0.5	129	49	242	58
FiM	1.3	7.5	335	-	335	-

TABLE I. Summary of the magnetic and electrical properties of Ni $_x$  and the single FiM sample at room temperature. From left to right:  $M_s t$  of the FiM,  $R_{AHE}$ , resistivity of Ni $_x$ , Ni $_x - r$ , and FiM layer, and current branching ratio in the  $Ni_xCu_{1-x}$  layer. For the Ni $_x$  samples,  $\rho_{FiM}$  was estimated using a parallel resistor model.

Based on the large charge-to-spin conversion efficiency,

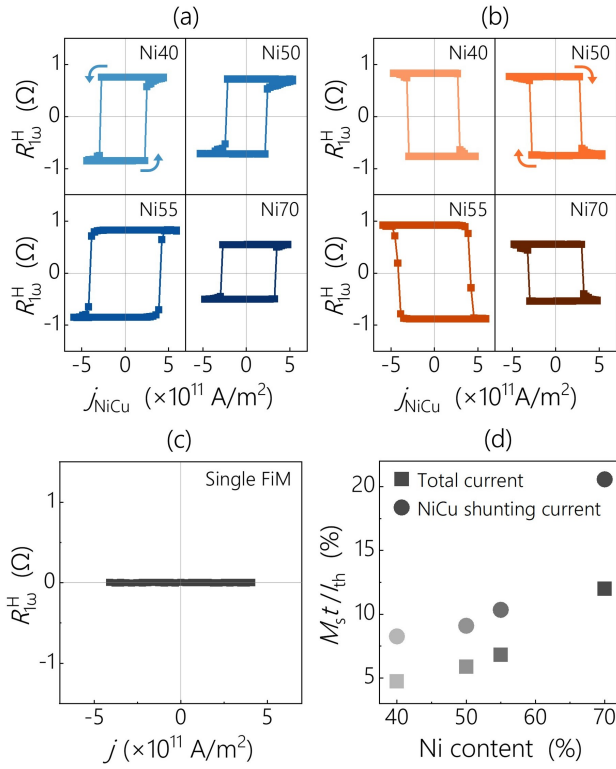


FIG. 3. SOT-induced magnetization switching. (a) and (b) Anomalous Hall resistance as a function of current density in  $Ni_xCu_{1-x}$ . The switching loops are acquired using 10-ms-long current pulses in the presence of an in-plane magnetic field of 10 mT oriented along (a)  $-x$  and (b)  $+x$ . (c) Anomalous Hall resistance as a function of current density for the single FiM sample. The loop is acquired using 10-ms-long current pulses and an in-plane magnetic field of 170 mT oriented along  $+x$ . (d) Ratio of the magnetic moment per unit area to the threshold switching current as a function of Ni content.

we further demonstrate SOT-induced magnetization switching of  $Ni_x$  for four different alloy's compositions ( $x = 40, 50, 55, 70\%$ ). To do so, we injected 10-ms-long current pulses to induce magnetization switching and inspected the magnetization state by reading  $R_{l\omega}^H$  using an alternate current of frequency  $\omega/(2\pi) = 115\text{Hz}$  after each pulse. As required for samples with perpendicular magnetic anisotropy, we apply an in-plane magnetic field to break the symmetry of the DL torque and define the switching polarity.<sup>2</sup> Figures 3(a) and (b) show the switching loops of  $Ni_x$  acquired for negative and positive external magnetic fields of amplitude 10mT applied along the  $x$ -axis. For all the samples, we observed full magnetization switching, as demonstrated by the semi-amplitude of the switching loops, matching the saturation  $R_{AHE}$  values. As expected, the switching polarity changes upon inversion of the in-plane magnetic field. In addition, the switching polarity is the same as observed in Pt/Co,<sup>2</sup> consistently with the sign of the SOTs. We further verified that switching occurs reliably using 100-ns-long current pulses and that the threshold switching current  $I_{th}$  decreases monotonically with the applied in-plane field. Measurements of the single FiM sample gave null results, as shown in Fig. 3(c), excluding the possibility of

switching induced by self-torques in the FiM material.<sup>58</sup>

$I_{th}$  is generally influenced by the coercivity and magnetic anisotropy of the FiM layer, which can vary from sample to sample. If such variations are neglected, the ratio  $M_s t / I_{th}$  can be taken as a rough measure of the SOT switching efficiency. Figure 3(d) shows that  $M_s t / I_{th}$  measured in the different  $Ni_x$  samples improves with increasing Ni content, in agreement with the trend of the SOT efficiency reported in Fig. 2(d). The same trend is observed if  $I_{th}$  is taken as the total current (squares) or only the current flowing in the  $Ni_xCu_{1-x}$  layer (dots). The improved switching efficiency at  $x = 70\%$  is also in agreement with the higher charge-to-spin conversion efficiency measured by ferromagnetic resonance.<sup>46</sup>

In conclusion, our results show that  $Ni_xCu_{1-x}$  alloys are very efficient generators of SOTs. Current injection in  $Ni_xCu_{1-x}$  is further shown to induce reliable switching of the magnetization of a 20-nm-thick [Gd/Fe] multilayer at a current density of about  $5 \times 10^{11} A/m^2$ . The SOT efficiency increases with Ni content, reaching a maximum spin Hall conductivity of  $\xi_{DL}^E = 1.04 \times 10^5 \Omega^{-1} m^{-1}$  in Ni55, which is comparable to that of heavy metal systems.

## ACKNOWLEDGMENTS

This work was supported by the Swiss National Science Foundation (Grant No. 200020-200465). P.N. acknowledges the support of the ETH Zurich Postdoctoral Fellowship Program 19-2 FEL-61. We thank Laura van Schie for her assistance in performing switching measurements using 100-ns-long current pulses.

The authors have no conflicts to disclose.

The data that support the findings of this study are openly available from the ETH Research Collection at <https://doi.org/10.3929/ethz-b-000633473>.

<sup>1</sup>A. Manchon, J. Železný, I. M. Miron, T. Jungwirth, J. Sinova, A. Thiaville, K. Garello, and P. Gambardella, "Current-induced spin-orbit torques in ferromagnetic and antiferromagnetic systems," *Rev. Mod. Phys.* **91**(3), 035004 (2019).

<sup>2</sup>I. M. Miron, K. Garello, G. Gaudin, P.-J. Zermatten, M. V. Costache, S. Auffret, S. Bandiera, B. Rodmacq, A. Schuhl, and P. Gambardella, "Perpendicular switching of a single ferromagnetic layer induced by in-plane current injection," *Nature* **476**, 189–193 (2011).

<sup>3</sup>L. Liu, C.-F. Pai, Y. Li, H. Tseng, D. Ralph, and R. Buhrman, "Spin-torque switching with the giant spin Hall effect of tantalum," *Science* **336**, 555 (2012).

<sup>4</sup>E. Grimaldi, V. Krizakova, G. Sala, F. Yasin, S. Couet, G. S. Kar, K. Garello, and P. Gambardella, "Single-shot dynamics of spin-orbit torque and spin transfer torque switching in three-terminal magnetic tunnel junctions," *Nat. Nanotechnol.* **15**, 111–117 (2020).

<sup>5</sup>J. Finley and L. Liu, "Spin-Orbit-Torque Efficiency in Compensated Ferromagnetic Cobalt-Terbium Alloys," *Phys. Rev. Appl.* **6**, 054001 (2016).

<sup>6</sup>L. Caretta, M. Mann, F. Büttner, K. Ueda, B. Pfau, C. M. Günther, P. Hessler, A. Churikova, C. Klose, M. Schneider, D. Engel, C. Marcus, D. Bono, K. Bagschik, S. Eisebitt, and G. S. D. Beach, "Fast current-driven domain walls and small skyrmions in a compensated ferrimagnet," *Nat. Nanotechnol.* **13**, 1154–1160 (2018).

<sup>7</sup>T. H. Pham, S.-G. Je, P. Vallobrá, T. Fache, D. Lacour, G. Malinowski, M. C. Cyrille, G. Gaudin, O. Boule, M. Hehn, J.-C. Rojas-Sánchez, and S. Mangin, "Thermal Contribution to the Spin-Orbit Torque in Metallic-Ferrimagnetic Systems," *Phys. Rev. Appl.* **9**, 064032 (2018).

- <sup>8</sup>G. Sala and P. Gambardella, “Ferrimagnetic Dynamics Induced by Spin-Orbit Torques,” *Adv. Mater. Interfaces* **9**, 2201622 (2022).
- <sup>9</sup>K. Olejník, T. Seifert, Z. Kašpar, V. Novák, P. Wadley, R. P. Campion, M. Baumgartner, P. Gambardella, P. Němec, J. Wunderlich, J. Sinova, P. Kužel, M. Müller, T. Kampfrath, and T. Jungwirth, “Terahertz electrical writing speed in an antiferromagnetic memory,” *Sci. Adv.* **4**, eaar3566 (2018).
- <sup>10</sup>H. Tsai, T. Higo, K. Kondou, T. Nomoto, A. Sakai, A. Kobayashi, T. Nakano, K. Yakushiji, R. Arita, S. Miwa, Y. Otani, and S. Nakatsuji, “Electrical manipulation of a topological antiferromagnetic state,” *Nature* **580**, 608–613 (2020).
- <sup>11</sup>G. K. Krishnaswamy, G. Sala, B. Jacot, C.-H. Lambert, R. Schlitz, M. D. Rossell, P. Noël, and P. Gambardella, “Time-Dependent Multistate Switching of Topological Antiferromagnetic Order in  $Mn_3Sn$ ,” *Phys. Rev. Appl.* **18**, 024064 (2022).
- <sup>12</sup>V. Krizakova, M. Perumkunnil, S. Couet, P. Gambardella, and K. Garello, “Spin-orbit torque switching of magnetic tunnel junctions for memory applications,” *J. Magn. Magn. Mater.* **562**, 169692 (2022).
- <sup>13</sup>R. Bläsing, A. A. Khan, P. C. Filippou, C. Garg, F. Hameed, J. Castrillon, and S. S. P. Parkin, “Magnetic Racetrack Memory: From Physics to the Cusp of Applications Within a Decade,” *Proc. IEEE* **108**, 1303–1321 (2020).
- <sup>14</sup>Z. Luo, A. Hrabec, T. P. Dao, G. Sala, S. Finizio, J. Feng, S. Mayr, J. Raabe, P. Gambardella, and L. J. Heyderman, “Current-driven magnetic domain-wall logic,” *Nature* **579**, 214–218 (2020).
- <sup>15</sup>V. E. Demidov, S. Urazhdin, G. de Loubens, O. Klein, V. Cros, A. Anane, and S. O. Demokritov, “Magnetization oscillations and waves driven by pure spin currents,” *Phys. Rep.* **673**, 1–31 (2017).
- <sup>16</sup>M. Zahedinejad, H. Fulara, R. Khymyn, A. Houshang, M. Dvornik, S. Fukami, S. Kanai, H. Ohno, and J. Åkerman, “Memristive control of mutual spin Hall nano-oscillator synchronization for neuromorphic computing,” *Nat. Mater.* **21**, 81–87 (2022).
- <sup>17</sup>C.-F. Pai, L. Liu, Y. Li, H. W. Tseng, D. C. Ralph, and R. A. Buhrman, “Spin transfer torque devices utilizing the giant spin Hall effect of tungsten,” *Appl. Phys. Lett.* **101** (2012).
- <sup>18</sup>K. Garello, I. M. Miron, C. O. Avci, F. Freimuth, Y. Mokrousov, S. Blügel, S. Auffret, O. Boulle, G. Gaudin, and P. Gambardella, “Symmetry and magnitude of spin-orbit torques in ferromagnetic heterostructures,” *Nat. Nanotechnol.* **8**, 587–593 (2013).
- <sup>19</sup>J. Kim, J. Sinha, M. Hayashi, M. Yamanouchi, S. Fukami, T. Suzuki, S. Mitani, and H. Ohno, “Layer thickness dependence of the current-induced effective field vector in Ta/CoFeB/MgO,” *Nat. Mater.* **12**, 240 (2013).
- <sup>20</sup>Y. Ishikuro, M. Kawaguchi, N. Kato, Y.-C. Lau, and M. Hayashi, “Dzyaloshinskii-Moriya interaction and spin-orbit torque at the Ir/Co interface,” *Phys. Rev. B* **99**, 134421 (2019).
- <sup>21</sup>I. M. Miron, G. Gaudin, S. Auffret, B. Rodmacq, A. Schuhl, S. Pizzini, J. Vogel, and P. Gambardella, “Current-driven spin torque induced by the Rashba effect in a ferromagnetic metal layer,” *Nat. Mater.* **9**, 230–234 (2010).
- <sup>22</sup>J. Sinova, S. O. Valenzuela, J. Wunderlich, C.-H. Back, and T. Jungwirth, “Spin Hall effects,” *Rev. Mod. Phys.* **87**, 1213 (2015).
- <sup>23</sup>G. Bihlmayer, P. Noël, D. V. Vyalikh, E. V. Chulkov, and A. Manchon, “Rashba-like physics in condensed matter,” *Nat. Rev. Phys.* **4**, 642–659 (2022).
- <sup>24</sup>M.-H. Nguyen, D. C. Ralph, and R. A. Buhrman, “Spin Torque Study of the Spin Hall Conductivity and Spin Diffusion Length in Platinum Thin Films with Varying Resistivity,” *Phys. Rev. Lett.* **116**, 126601 (2016).
- <sup>25</sup>B. F. Miao, Y. Huang, D. Qu, and C. L. Chien, “Inverse Spin Hall Effect in a Ferromagnetic Metal,” *Phys. Rev. Lett.* **111**, 066602 (2013).
- <sup>26</sup>C. Du, H. Wang, F. Yang, and P. C. Hammel, “Systematic variation of spin-orbit coupling with d-orbital filling: Large inverse spin Hall effect in 3d transition metals,” *Phys. Rev. B* **90**, 140407(R) (2014).
- <sup>27</sup>D. Qu, S. Y. Huang, and C. L. Chien, “Inverse spin Hall effect in Cr: Independence of antiferromagnetic ordering,” *Phys. Rev. B* **92**, 020418(R) (2015).
- <sup>28</sup>H. An, Y. Kageyama, Y. Kanno, N. Enishi, and K. Ando, “Spin-torque generator engineered by natural oxidation of Cu,” *Nat. Commun.* **7**, 13069 (2016).
- <sup>29</sup>T. Wang, W. Wang, Y. Xie, M. A. Warsi, J. Wu, Y. Chen, V. O. Lorenz, X. Fan, and J. Q. Xiao, “Large spin Hall angle in vanadium film,” *Sci. Rep.* **7**, 1306 (2017).
- <sup>30</sup>S. H. C. Baek, V. P. Amin, Y.-W. Oh, G. Go, S.-J. Lee, G.-H. Lee, K.-J. Kim, M. D. Stiles, B.-G. Park, and K.-J. Lee, “Spin currents and spin-orbit torques in ferromagnetic trilayers,” *Nat. Mater.* **17**, 509–513 (2018).
- <sup>31</sup>Y. Hibino, T. Taniguchi, K. Yakushiji, A. Fukushima, H. Kubota, and S. Yuasa, “Large Spin-Orbit-Torque Efficiency Generated by Spin Hall Effect in Paramagnetic Co-Ni-B Alloys,” *Phys. Rev. Appl.* **14**, 064056 (2020).
- <sup>32</sup>H. Kontani, T. Tanaka, D. S. Hirashima, K. Yamada, and J. Inoue, “Giant Orbital Hall Effect in Transition Metals: Origin of Large Spin and Anomalous Hall Effects,” *Phys. Rev. Lett.* **102**, 016601 (2009).
- <sup>33</sup>D. Jo, D. Go, and H.-W. Lee, “Gigantic intrinsic orbital hall effects in weakly spin-orbit coupled metals,” *Phys. Rev. B* **98**, 214405 (2018).
- <sup>34</sup>D. Go, F. Freimuth, J.-P. Hanke, F. Xue, O. Gomonay, K.-J. Lee, S. Blügel, P. M. Haney, H.-W. Lee, and Y. Mokrousov, “Theory of current-induced angular momentum transfer dynamics in spin-orbit coupled systems,” *Phys. Rev. Res.* **2**, 033401 (2020).
- <sup>35</sup>D. Lee, D. Go, H.-J. Park, W. Jeong, H.-W. Ko, D. Yun, D. Jo, S. Lee, G. Go, J. H. Oh, K.-J. Kim, B.-G. Park, B.-C. Min, H. C. Koo, H.-W. Lee, O. Lee, and K.-J. Lee, “Orbital torque in magnetic bilayers,” *Nat. Commun.* **12**, 6710 (2021).
- <sup>36</sup>S. Lee, M.-G. Kang, D. Go, D. Kim, J.-H. Kang, T. Lee, G.-H. Lee, J. Kang, N. J. Lee, Y. Mokrousov, S. Kim, K.-J. Kim, K.-J. Lee, and B.-G. Park, “Efficient conversion of orbital Hall current to spin current for spin-orbit torque switching,” *Commun. Phys.* **4**, 234 (2021).
- <sup>37</sup>G. Sala and P. Gambardella, “Giant orbital Hall effect and orbital-to-spin conversion in 3d, 5d, and 4f metallic heterostructures,” *Phys. Rev. Res.* **4**, 033037 (2022).
- <sup>38</sup>L. Zhu, D. C. Ralph, and R. A. Buhrman, “Maximizing spin-orbit torque generated by the spin Hall effect of Pt,” *Appl. Phys. Rev.* **8** (2021).
- <sup>39</sup>C.-Y. Hu and C.-F. Pai, “Benchmarking of Spin-Orbit Torque Switching Efficiency in Pt Alloys,” *Adv. Quantum Technol.* **3**, 2000024 (2020).
- <sup>40</sup>Z. Chi, Y.-C. Lau, M. Kawaguchi, and M. Hayashi, “Charge-spin conversion in Pt<sub>1-x</sub>Bix alloys for spin-orbit torque switching,” *APL Mater.* **9** (2021).
- <sup>41</sup>P. Wang, A. Migliorini, S.-H. Yang, J.-C. Jeon, I. Kostanovskiy, H. Meyerheim, H. Han, H. Deniz, and S. S. P. Parkin, “Giant Spin Hall Effect and Spin-Orbit Torques in 5d Transition Metal-Aluminum Alloys from Extrinsic Scattering,” *Adv. Mater.* **34**, 2109406 (2022).
- <sup>42</sup>Y. Niimi, Y. Kawanishi, D. H. Wei, C. Deranlot, H. X. Yang, M. Chshiev, T. Valet, A. Fert, and Y. Otani, “Giant Spin Hall Effect Induced by Skew Scattering from Bismuth Impurities inside Thin Film CuBi Alloys,” *Phys. Rev. Lett.* **109**, 156602 (2012).
- <sup>43</sup>L. Zhu, D. C. Ralph, and R. A. Buhrman, “Highly Efficient Spin-Current Generation by the Spin Hall Effect in Au<sub>1-x</sub>Pt<sub>x</sub>,” *Phys. Rev. Appl.* **10**, 031001 (2018).
- <sup>44</sup>R. M. Bozorth, *Ferromagnetism* (Wiley, New York, 1993).
- <sup>45</sup>S. A. Ahern, M. J. C. Martin, and W. Sucksmith, “The spontaneous magnetization of nickel + copper alloys,” *Proc. R. Soc. Lond. A* **248**, 145–152 (1958).
- <sup>46</sup>M. W. Keller, K. S. Gerace, M. Arora, E. K. Delczeg-Czirjak, J. M. Shaw, and T. J. Silva, “Near-unity spin Hall ratio in Ni<sub>x</sub>Cu<sub>1-x</sub> alloys,” *Phys. Rev. B* **99**, 214411 (2019).
- <sup>47</sup>S. Varotto, M. Cosset-Chéneau, C. Grèzes, Y. Fu, P. Warin, A. Brenac, J.-F. Jacquot, S. Gambarelli, C. Rinaldi, V. Baltz, J.-P. Attané, L. Vila, and P. Noël, “Independence of the Inverse Spin Hall Effect with the Magnetic Phase in Thin NiCu Films,” *Phys. Rev. Lett.* **125**, 267204 (2020).
- <sup>48</sup>P.-H. Wu, D. Qu, Y.-C. Tu, Y.-Z. Lin, C. Chien, and S.-Y. Huang, “Exploiting Spin Fluctuations for Enhanced Pure Spin Current,” *Phys. Rev. Lett.* **128**, 227203 (2022).
- <sup>49</sup>H. Cheng, Y. Wang, H. He, Q. Huang, and Y. Lu, “Efficient and temperature-independent terahertz emission from CoFeB/NiCu heterostructures,” *Phys. Rev. B* **105**, 155141 (2022).
- <sup>50</sup>C. O. Avci, K. Garello, M. Gabureac, A. Ghosh, A. Fuhrer, S. F. Alvarado, and P. Gambardella, “Interplay of spin-orbit torque and thermoelectric effects in ferromagnet/normal-metal bilayers,” *Phys. Rev. B* **90**, 224427 (2014).
- <sup>51</sup>Y. Omori, E. Sagasta, Y. Niimi, M. Gradhand, L. E. Hueso, F. Casanova, and Y. Otani, “Relation between spin Hall effect and anomalous Hall effect in 3d ferromagnetic metals,” *Phys. Rev. B* **99**, 014403 (2019).
- <sup>52</sup>E. Haltz, R. Weil, J. Sampaio, A. Pointillon, O. Rousseau, K. March,

- N. Brun, Z. Li, E. Briand, C. Bachelet, Y. Dumont, and A. Mougin, "Deviations from bulk behavior in TbFe(Co) thin films: Interfaces contribution in the biased composition," *Phys. Rev. Mater.* **2**, 104410 (2018).
- <sup>53</sup>Q. Zhang, D. Zheng, Y. Wen, Y. Zhao, W. Mi, A. Manchon, O. Boulle, and X. Zhang, "Effect of surface roughness on the anomalous Hall effect in Fe thin films," *Phys. Rev. B* **101**, 134412 (2020).
- <sup>54</sup>T. H. Dang, Q. Barbedienne, D. Q. To, E. Rongione, N. Reyren, F. Godel, S. Collin, J. M. George, and H. Jaffrès, "Anomalous Hall effect in  $3d/5d$  multilayers mediated by interface scattering and nonlocal spin conductivity," *Phys. Rev. B* **102**, 144405 (2020).
- <sup>55</sup>J. Bello, D. Lacour, S. Migot, J. Ghanbaja, S. Mangin, and M. Hehn, "Impact of interfaces on magnetic properties of  $\text{Gd}_x(\text{Fe}_{90}\text{Co}_{10})_{1-x}$  alloys," *Appl. Phys. Lett.* **121**, 212402 (2022).
- <sup>56</sup>M. Hayashi, J. Kim, M. Yamanouchi, and H. Ohno, "Quantitative characterization of the spin-orbit torque using harmonic Hall voltage measurements," *Phys. Rev. B* **89**, 144425 (2014).
- <sup>57</sup>S.-Y. Hsu, P. Holody, R. Loloee, J. M. Rittner, W. P. Pratt, and P. A. Schroeder, "Spin-diffusion lengths of  $\text{Cu}_{1-x}\text{Ni}_x$  using current perpendicular to plane magnetoresistance measurements of magnetic multilayers," *Phys. Rev. B* **54**, 9027 (1996).
- <sup>58</sup>D. Céspedes-Berrocá, H. Damas, S. Petit-Watelot, D. Maccariello, P. Tang, A. Arriola-Córdova, P. Vallobrá, Y. Xu, J.-L. Bello, E. Martín, S. Migot, J. Ghanbaja, S. Zhang, M. Hehn, S. Mangin, C. Panagopoulos, V. Cros, A. Fert, and J.-C. Rojas-Sánchez, "Current-Induced Spin Torques on Single GdFeCo Magnetic Layers," *Adv. Mater.* **33**, 2007047 (2021).